

Decadal trends of MERRA-estimated PM_{2.5} concentrations in East Asia and potential exposure from 1990 to 2019

Shuai Yin

Earth System Division, National Institute for Environmental Studies, Tsukuba, 3058506, Japan



HIGHLIGHTS

- Before 2000, PM_{2.5} concentrations varied little in EA.
- From 2000 to 2009, the air quality substantially deteriorated over the entire study region.
- Since 2013, implementing of APPCAP effectively controlled PM_{2.5} pollution in EA.
- Because of population aging, EA will face more serious challenges in air quality management.

ARTICLE INFO

Keywords:
AOD
North China Plain
Population aging
Sulfate
Theil-Sen median

ABSTRACT

Because of their long temporal coverage, MERRA-2 data were used to estimate PM_{2.5} concentrations over east Asia (EA), and those data were integrated with population information to comprehensively assess exposure from 1990 to 2019. Theil-Sen median trend and geographic distribution analyses were conducted to characterize the spatiotemporal variations in regional PM_{2.5} concentrations. The results indicated that anthropogenic aerosol concentrations were much higher in the fast-growing and densely populated eastern and southern parts of China. Before 2000, PM_{2.5} concentrations varied little in most areas, and they only notably increased during 1990–1999 in southern China and South Korea. At that time, 88% of EA's population was exposed to lower levels of PM_{2.5} pollution (annual PM_{2.5} ≤ 35 µg/m³). From 2000 to 2009, the air quality substantially deteriorated over the entire study region, and the rates of increase of the population-weighted PM_{2.5} concentration reached 1.6 (1.1–1.9) µg/m³/yr in east China and 1.4 (1.1–1.6) µg/m³/yr in south China. Almost 50% of the population was exposed to the highest level (Level 5) of pollution (annual PM_{2.5} > 35 µg/m³). To combat air pollution, the State Council of China promulgated the toughest-ever Air Pollution Prevention and Control Action Plan in 2013, which effectively decreased PM_{2.5} concentrations in the heavily polluted east and south China. As the air quality improved, the population exposed to annual PM_{2.5} concentrations of <35 µg/m³ returned to 63.5% in 2018. An age-group analysis indicated that, even with decreasing levels of pollution, the older adult (≥65 years old) population exposed to Level 5 pollution peaked in 2019 at 83.1 million. This implies that, as the issue of population aging becomes increasingly important in EA, additional strict control of primary PM_{2.5} and precursor emissions will be required to help decrease the pollution-related health risks facing residents of EA.

1. Introduction

In the past few decades, ambient particulate matter, especially PM_{2.5} (diameter ≤ 2.5 µm), has become a major threat to human health. Given its small size, PM_{2.5} is likely to penetrate through lung cells into circulating blood, and numerous epidemiological studies have revealed the robust association between long-term exposure to high concentrations of PM_{2.5} and premature mortality from ischemic heart disease, stroke, lung cancer, chronic obstructive pulmonary disease, and respiratory

infections (Ghude et al., 2016; Laden et al., 2000; Maji et al., 2018; Lu et al., 2015). Compared with coarser ambient air particulate matter, PM_{2.5} is less affected by wet deposition and sometimes can remain in the atmosphere for several weeks, which is likely to induce severe pollution episodes in non-source regions through long-range transport (Li et al., 2017; Kaneyasu et al., 2014). From 1990 to 2013, global population-weighted PM_{2.5} concentrations increased by more than 20% (Brauer et al., 2016), and the World Health Organization (WHO) estimates that over 92% of the world's population lived in areas that

E-mail address: yin.shuai@nies.go.jp.

exceeded its Air Quality Guidelines (AQG: 10 $\mu\text{g}/\text{m}^3$). Ambient PM_{2.5} pollution is an essential societal issue, particularly in fast-developing regions in Asia, where rapid urbanization and industrialization have significantly increased primary PM_{2.5} emissions. Anthropogenic emissions of secondary PM_{2.5} precursor species (e.g., nitrogen oxides [NO_x], sulfur oxides [SO_x], and volatile organic compounds) have also contributed to urban haze pollution. According to the 2015 Global Burden of Disease (GBD) assessment, exposure to ambient PM_{2.5} caused 4.2 million deaths globally and 103.1 million disability-adjusted life-years, ranking as the fifth leading risk factor for premature mortality globally; 59% of the deaths occurred in east and south Asia (Cohen et al., 2017).

Meteorological monitoring stations are widespread and have a long history, whereas the monitoring network of air quality is still small-scale, and the monitoring time span is extremely limited. These issues are even more prominent in the developing countries, which often suffer from severe air pollution. For example, PM_{2.5} has only been incorporated into China's National Ambient Air Quality Standards (NAAQS GB3095-2012) since February 2012 (Zhang and Cao, 2015). Before that, PM_{2.5} was monitored only in the well-developed regions of China, such as the Yangtze River Delta and Pearl River Delta regions and provincial capitals. Monitoring was extended to every prefecture-level city in China in 2015, which means China had no nationwide PM_{2.5} monitoring data before 2015.

With the development of remote-sensing and data-retrieval technology, Earth-observing satellites have become a powerful tool to monitor surface aerosol characteristics; one widely used proxy for estimating PM_{2.5} concentration is aerosol optical depth (AOD). This method overcomes the barriers in obtaining PM_{2.5} concentrations over a long time span and with large spatial coverage, especially for regions with no ground measurements. A large number of early studies used simple empirical relationships to estimate surface PM_{2.5} from total-column AOD (Wang and Christopher, 2003; Liu et al., 2004); however, this method requires sufficient ground-measurement data to establish the relevant relationships and reduce uncertainties (Shao et al., 2017). More recent studies have incorporated data on land use, topography, population, and meteorology to better relate PM_{2.5} and AOD; they have also included the use of geographical weighted regression (GWR) and land use regression (LUR) (Stieb et al., 2016; Song et al., 2014; You et al., 2016).

Satellite observations have discontinuous spatiotemporal coverage because of cloud contamination, retrieval uncertainties, and data gaps among heterogeneous sensors. One approach to compensate the inherent shortcomings of remote-sensing data and provide a better representation of ambient aerosols is to optimize the advantages of models and satellite observations by using data assimilation techniques. Several research groups have developed aerosol data assimilation capabilities on a global scale (Zhang et al., 2008; Benedetti et al., 2009; Sekiyama et al., 2010). One of the most well-known is the Modern-Era Retrospective Analysis for Research and Applications (MERRA), which was implemented by NASA's Global Modeling and Assimilation Office with two primary goals: to place the observations from NASA's satellites into a climate context and to improve upon the hydrologic cycle that was determined by earlier generations of reanalysis (Rienecker et al., 2011). The temporal coverage of MERRA is over 40 years, and it provides abundant data for global aerosol studies.

Despite using ground-measured or remote-sensing datasets, most previous studies have focused on PM_{2.5} pollution after 2010, and there are few long-term studies (i.e., over several decades). In this study, MERRA aerosol data were used to estimate PM_{2.5} concentration over East Asia for the past 30 years (1990–2019). The interannual variation and spatiotemporal characteristics of PM_{2.5} and several aerosol types were explored on various spatial scales. MERRA data were also integrated with dynamic demographic data to reveal variations in the population and age groups exposed to high PM_{2.5} concentrations. The results will aid in increasing our understanding of the characteristics of

long-term trends of PM_{2.5} over East Asia (EA). They should also be useful in verifying whether the countermeasures and policy-making of local governments have positively mitigated urban air pollution, which is essential knowledge to design effective strategies and further reduce PM_{2.5} concentrations in the future.

2. Datasets and methodology

2.1. Datasets

2.1.1. PM_{2.5} concentration

MERRA-2 is NASA's latest reanalysis dataset and has provided data since 1980; it uses the Goddard Earth Observing System, version 5 (GEOS-5) Earth system model. It includes assimilation of bias-corrected AOD from the Moderate Resolution Imaging Spectroradiometer (MODIS) and Advanced Very High Resolution Radiometer (AVHRR), non-bias-corrected AOD from the space-based Multiangle Imaging SpectroRadiometer (MISR), and ground-measured AOD from Aerosol Robotic Network (AERONET) stations (Buchard et al., 2017). It covers remote-sensing data from 1980 to the present and assimilates satellite and ground-measured data with a spatial resolution of $0.5^\circ \times 0.625^\circ$. MERRA-2 has several remarkable improvements, including incorporating new observations not available for MERRA-1 and reducing spurious trends and jumps related to changes in the meteorological observation system (McCarty et al., 2016; Randles et al., 2017). MERRA-2 provides the concentrations of five types of aerosols: dust (DS), sea salt (SS), black carbon (BC), organic carbon (OC), and sulfate (SO₄). Buchard et al. (2016) proposed a method to estimate surface PM_{2.5} concentrations from MERRA products. In this section, we use that method to explore the changes in concentrations and spatial distributions of PM_{2.5} over EA from 1990 to 2019. The following equation was used:

$$\text{PM}_{2.5} = [\text{Dust}_{2.5}] + [\text{SS}_{2.5}] + [\text{BC}] + 1.4 \times [\text{OC}] + 1.375 \times [\text{SO}_4] \quad (1)$$

where [Dust_{2.5}], [SS_{2.5}], [BC], [OC], and [SO₄] are the concentrations of dust, sea-salt, black carbon, organic carbon and sulfate particulate, respectively, all of which have diameters less than or equal to 2.5 μm .

2.1.2. Population

Demographic data were derived from the Gridded Population of the World (GPW) and Population Division of United Nations (UN). GPW was developed by the Center for International Earth Science Network (CIESIN) at Columbia University, and the first version was released in 1995. For the latest version (GPWv4), population input data were collected from the results of the 2010 round of Population and Housing Censuses, which took place between 2005 and 2014 (Doxsey-Whitfield et al., 2015). GPWv4 provides a global population map for the years 2000, 2005, 2010, 2015, and 2020; gridded population data for 1990 and 1995 were obtained from GPWv3. The population distribution maps in other study years were linearly extrapolated by using GPWv3 and GPWv4 as a basis. Because GPWv3 and GPWv4 were not developed using updated census information, annual population data collected from the UN Population Division for four countries (China, Japan, South Korea, and North Korea) were used to adjust the extrapolation results. Meanwhile, population pyramid data of the four countries were also derived from UN Population Division data to elaborate on the exposure of PM_{2.5} on different age groups.

2.1.3. Emission inventories

Since surface PM_{2.5} concentration are highly influenced by natural and anthropogenic emission, two widely used emission inventories are adopted to explore the effect of emission on interannual variation of PM_{2.5} in EA. One is the Global Fire Emissions Database (GFED), which is developed to help elucidate the role of biomass burning in the global carbon cycle and within the Earth system as a whole (Giglio et al., 2013;

(Randerson et al., 2012; van der Werf et al., 2010). GFED combines fire activity and vegetation productivity information from several satellite sensors to estimate globally gridded monthly burned area and fire emissions. The current version 4.1s has a $0.25^\circ \times 0.25^\circ$ spatial resolution and the data including fire carbon emissions and dry matter emissions are available from 1997 onward (van der Werf et al., 2017). In this study, the fractional contributions of different fire types from GFED are combined with recommended emission factors (mostly based on Akagi et al., 2011) to estimate CO₂ and PM_{2.5} emission from biomass burning (refer to Section 2 in supplementary material). The anthropogenic emission is obtained from Emission Database for Global Atmosphere Research (EDGAR). EDGAR compiles anthropogenic emissions for greenhouse gases, and for multiple air pollutants based on international statistics and best-available emission factors (Crippa et al., 2018; Janssens-Maenhout et al., 2019). EDGAR data provide sufficient support for atmospheric modeling and for mitigation scenario and as well as for policy evaluation (Crippa et al., 2020). In this study annual anthropogenic emission of CO₂ and PM_{2.5} in EA is obtained from EDGAR version 6.0 and version 5.0. Two versions of the datasets both have a spatial resolution of $0.1^\circ \times 0.1^\circ$ and they provide the anthropogenic emission data of greenhouse gases from 1970 to 2018 and air pollutants from 1970 to 2015, respectively.

2.2. Methodology

Trend analysis is an indispensable tool in temporal dynamic analyses to explore and quantify interannual variations. Although, the linear trend is widely used in most studies, it is sensitive to outliers and only applicable to normally distributed data. Because air pollutant concentrations are always non-normally distributed (Munir et al., 2013), non-parametric statistical tests were used in this study. Theil-Sen median analysis is a robust non-parametric statistical method that is highly effective for assessing the rate of change in short series (Theil, 1950; Sen, 1968; Hoaglin et al., 2000). The Theil-Sen median trend calculates the median slopes between all pair-wise combinations of time-series data; it is resistant to outliers and tends to accurately calculate the slope, even for non-normal data (Vanem and Walker, 2013). The Theil-Sen median slope is calculated by the following equation:

$$\text{Slope} = \text{Median}\left(\frac{x_i - x_j}{t_i - t_j}\right) \quad (2)$$

Where x_i and x_j are the PM_{2.5} concentrations at time t_i and t_j ($i > j$), respectively.

Two types of geographic distribution analysis, standard deviation ellipse (SDE) and median center (MEC), were used to summarize the spatial characteristics of PM_{2.5} concentrations. SDE was first proposed by Lefever (1926). It calculates the standard distance of a set of discrete points from the average center and results in an ellipse in which the two main directions usually delineate the overall characteristics of geo-spatial distributions. MEC analysis uses an iterative algorithm to explore the location of a point that minimizes the Euclidean distance to all features in the datasets. By comparing the variation of SDE and MEC across a time series, it was possible to reveal the dynamic spatial variation of PM_{2.5} in EA over the past three decades.

PM_{2.5} data estimated by MERRA-2 were spatially integrated with demographic data to explore variations among the population and age groups living at various pollution levels. In situ measured PM_{2.5} data from various sources (e.g., China's National Environmental Monitoring Center and WHO reports) were compared with PM_{2.5} data estimated from MERRA-2 to reveal any differences between these two datasets and to verify whether the PM_{2.5} concentrations estimated by MERRA-2 were significantly correlated to the ground observations.

3. Results and discussions

3.1. Spatial patterns and interannual variation of PM_{2.5}

3.1.1. The five kinds of aerosols

Owing to its heterogeneous population density, anthropogenic emissions, and climatic and topographical conditions, China was divided into four parts (east, west, north, and south) to illustrate the spatial characteristics of PM_{2.5} (see Fig. S-1 in the supplementary material). Fig. 1 shows the spatial patterns of the five kinds of aerosols and PM_{2.5} concentration across the study region. BC, OC, and SO₄ are typical anthropogenic aerosols, and their spatial distributions over the study area are somewhat similar to each other. The concentrations of these three anthropogenic aerosols in the North China Plain, Yangtze Plain, and Sichuan Basin (Fig. 1a–c), each of which is characterized by fast development, a large urban agglomeration, and a dense population, are much higher than the other regions. Refer to Fig. S-2 in the supplementary material for detailed information on the topography of China. BC aerosols are emitted from the incomplete combustion of fossil fuels, biofuel, and biomass (Chen et al., 2001; Cooke and Wilson, 1996; Lioussse et al., 1996). OC, which has both primary and secondary origins, accounts for a major fraction of fine-mode carbonaceous aerosols (Turpin et al., 2000). The OC concentration across the entire study area was much higher than the BC concentration (Table 1, Fig. 2d). The main source of SO₄ aerosols is anthropogenic sulfur dioxide (SO₂) emissions from the burning of fossil fuels (IPCC, 2007). Both during emission and while in the atmosphere, gaseous SO₂ can become oxidized to form SO₄ aerosols. Together, BC, OC, and SO₄ constituted approximately 75% of the aerosols in east, south China and the Korean Peninsula; whereas they accounted for only 7% and 41%, respectively, in the less populated west and north China (Table 1). Moreover, EDGAR revealed that the annual anthropogenic emission of CO₂ and PM_{2.5} in south and east China is much higher than in other regions, while the emission in west China is the lowest (Fig. S-3 and Tables S-2). Before 2000, the sum of BC, OC, and SO₄ concentrations in China was always below 8 µg/m³ (Fig. 2a). With China's economic rise and corresponding surge of fossil fuel consumption, the total concentration increased gradually and peaked at 11.5 µg/m³ in 2008. Fig. S-4 in the supplementary material shows that this increasing trend was even more prominent in east and south China, where the total concentrations peaked at 27.9 µg/m³ and 21.1 µg/m³, respectively, in 2011.

By contrast, the annual BC, OC, and SO₄ concentrations in Japan were relatively stable, fluctuating between 7 and 8 µg/m³ over the three decades (Fig. 2b). The interannual variation of the anthropogenic aerosols in Korean Peninsula was similar to that of China and is assumed to be closely related to long-range transported air pollutants emitted from China or other regions (Fig. 2c). Many studies have revealed that anthropogenic aerosols and natural dust aerosols originating in China can easily be transported by westerly winds to receptor areas (Lee et al., 2013; Oh et al., 2015; Onishi et al., 2012).

The interannual variation of OC concentrations was much greater in north China than in other regions (Fig. S-4c). In addition to anthropogenic emissions, another predominant source of OC aerosol is biomass burning (Hallquist et al., 2009), and the OC concentration was also high in Siberia, Southeast Asia, and the Indo-Gangetic Plain (Fig. 1b). GFED inventory shows that these regions are characterized by intense biomass burning (Fig. S-5). Unlike other regions in EA, the air quality and OC concentration in north China is highly influenced by biomass burning in Mongolia and forest fires in Siberia (Fig. S-4c, Fig. S-6 and Fig. S-7). In 1996, biomass burning occurred frequently in Mongolia, and the area affected by the burning was 10.2 million ha (Goldammer, 2001). Simultaneously, the concentration of OC aerosols in north China rose to 4.8 µg/m³, the second highest level during the study period. Although, no intense indigenous biomass burning was observed in 2003, in the spring of that year, boreal forest fires occurred in central and southern Siberia; in total, these fires were recorded as one of the largest forest fire

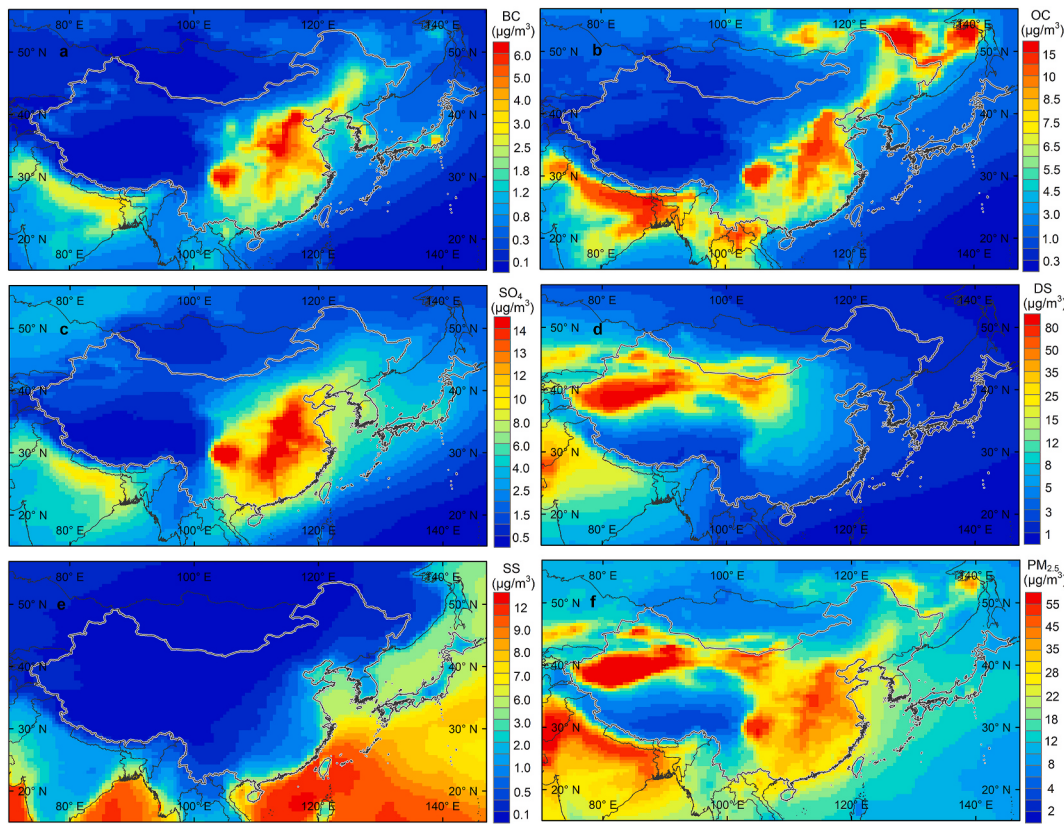


Fig. 1. The multiannual average concentration of the five types of aerosols and the estimated $\text{PM}_{2.5}$ concentrations over EA, 1990–2019: (a) BC, (b) OC, (c) SO_4 , (d) DS, (e) SS, and (f) $\text{PM}_{2.5}$.

Table 1

The average concentration of the five types of aerosols and $\text{PM}_{2.5}$ from 1990 to 2019 (unit: $\mu\text{g}/\text{m}^3$); average population-weighted (PW) $\text{PM}_{2.5}$ is also shown.

Region		BC	OC	SO_4	DS	SS	Average $\text{PM}_{2.5}$	PW $\text{PM}_{2.5}$
China	East	3.7 (± 0.2)	7.3 (± 0.4)	10.8 (± 1.1)	6.7 (± 0.3)	0.7 (± 0.1)	36.4 (± 2.3)	39.5 (± 2.7)
	South	2.0 (± 0.1)	5.8 (± 0.2)	8.9 (± 0.8)	3.9 (± 0.2)	0.9 (± 0.1)	27.3 (± 1.6)	32.7 (± 2.0)
	North	0.8 (± 0.1)	3.4 (± 0.6)	3.1 (± 0.2)	10.3 (± 0.3)	0.1 (± 0.0)	20.3 (± 1.1)	21.8 (± 1.3)
	West	0.1 (± 0.0)	0.5 (± 0.0)	0.9 (± 0.0)	21.3 (± 0.8)	0.1 (± 0.0)	23.5 (± 0.8)	29.7 (± 1.3)
	Nationwide	1.2 (± 0.1)	3.3 (± 0.2)	4.5 (± 0.4)	12.5 (± 0.4)	0.4 (± 0.0)	25.0 (± 1.0)	33.9 (± 2.1)
Japan		1.0 (± 0.0)	1.6 (± 0.2)	4.2 (± 0.1)	1.6 (± 0.1)	2.7 (± 0.1)	13.3 (± 0.4)	15.4 (± 0.4)
Korean Peninsula		1.5 (± 0.1)	3.0 (± 0.4)	6.5 (± 0.3)	2.5 (± 0.2)	1.3 (± 0.0)	18.3 (± 1.0)	20.9 (± 1.1)

Note: Numbers in the parentheses refer to the 95% confidence intervals.

events in Siberia in the past several decades (Jeong et al., 2008). Fig. S-7 indicates that annual CO_2 and $\text{PM}_{2.5}$ emission from biomass burning within south Siberia reached 6.8×10^8 and 6.5×10^6 ton in 2003, which are the highest from 1997 to 2019. The aerosols from this boreal forest fire not only affected regional air quality, but also had a notable effect on other countries, reaching as far as the west coast of North America (Lee et al., 2005; Kaneyasu et al., 2007; Murayama et al., 2004; Ikemori et al., 2015; Bertschi and Jaffe, 2005; Jaffe et al., 2004). Similarly, the results of this study show that the OC concentration of north China rose sharply to $9.7 \mu\text{g}/\text{m}^3$ in 2003 (Fig. S-4c), approximately three times the interannual average from 1990 to 2019. The annual OC concentration also increased in Japan and Korean Peninsula in 2003 (Fig. 2b and c).

The spatial distributions of the two natural aerosols, DS and SS, were completely different from those of BC, OC, and SO_4 . For example, the DS concentration was much higher in the southern part of the Xinjiang Uygur Autonomous Region and western Inner Mongolia (Fig. 1d). These regions are characterized by an arid climate and little vegetation cover. Two of Asia's largest deserts, the Taklimakan Desert and the Gobi Desert, are located in these regions. Table 1 shows that DS was the dominant aerosol in north and west China, making up 58% and 93% of

total regional aerosols, respectively. In spring, strong winds uplift massive amounts of DS aerosols from these arid areas, and they can be transported to east China, Korean Peninsula, Japan, and even to the west coast of North America (Chung, 1992; Zhang et al., 1993; Yu et al., 2006; Husar et al., 2001).

The SS concentration in EA is much lower than that of other types of aerosols, but it is always present in high concentrations in coastal regions (Fig. 1e). As the only island country in EA, Japan had the highest SS concentration, and its interannual average concentration reached $2.7 \mu\text{g}/\text{m}^3$, second only to SO_4 . High SS concentrations were also found in Korean Peninsula ($1.3 \mu\text{g}/\text{m}^3$).

3.1.2. $\text{PM}_{2.5}$ concentration

The estimated $\text{PM}_{2.5}$ concentrations were much higher in the fast-developing North China Plain, Yangtze Plain, and Sichuan Basin (dominated by anthropogenic aerosols) as well as in the arid Tarim Basin and Gobi region (dominated by DS aerosols) (Fig. 1f). To illustrate population exposure to air pollution, the regional population-weighted (PW) $\text{PM}_{2.5}$ concentration was also calculated, which reflects the estimated annual mean exposure level of an average resident to outdoor

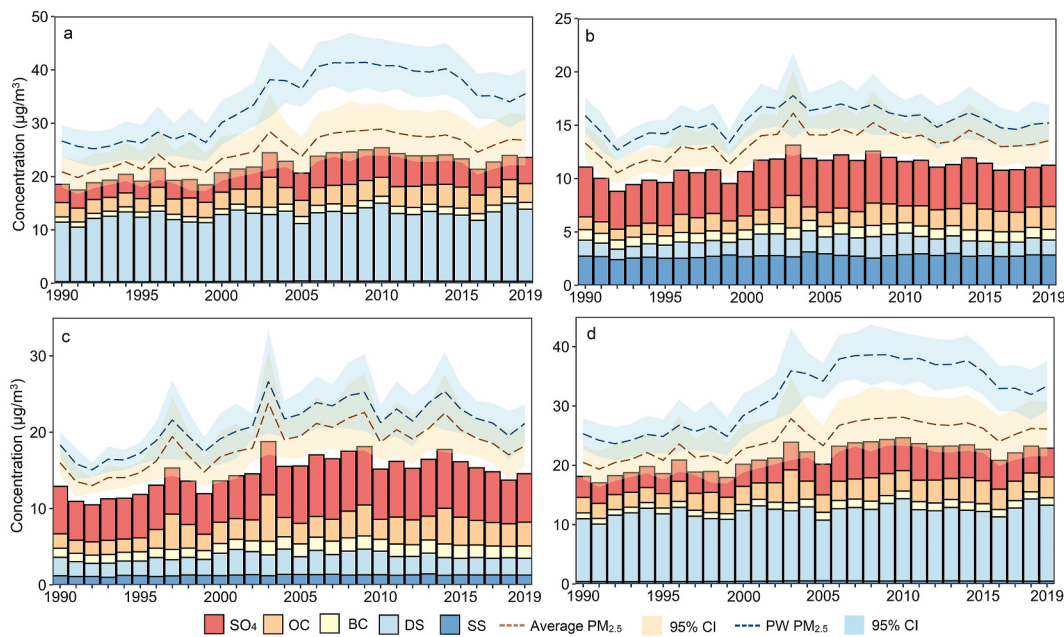


Fig. 2. The interannual variation of aerosols, PM_{2.5} and PW PM_{2.5} concentration in (a) China; (b) Japan; (c) Korean Peninsula, and (d) EA.

PM_{2.5}. The PW PM_{2.5} concentration in China was 33.9 µg/m³ across the study period, much higher than the average PM_{2.5} (25.0 µg/m³). East and south China are the most intensely populated regions in EA, and their combined population makes up 85% of the Chinese population and 74% of EA's population. Since 2000, air quality has substantially deteriorated in east and south China, which increased the gap between China's PW PM_{2.5} and average PM_{2.5}; in 2006, the gap reached 13.3 µg/m³ (Fig. 2a). The PW PM_{2.5} in Japan and Korea Peninsula was approximately 2.0 µg/m³ higher than their average PM_{2.5}. Unlike in China, the gap between the two PM indicators did not vary dramatically from 1990 to 2019 (Fig. 2b and c).

Table 1 and Fig. S-4a indicate that the average PM_{2.5} and PW PM_{2.5} concentrations were highest in east China, followed by south and west China. Before 2000, the average PM_{2.5} concentration in China ranged from 19.8 to 24.2 µg/m³, and the PW PM_{2.5} concentration ranged from 25.2 to 28.3 µg/m³. In the following years, the average and PW PM_{2.5} concentrations both gradually increased; eventually, the average PM_{2.5} concentration peaked at 28.9 µg/m³ in 2010, and the PW PM_{2.5} concentration peaked at 41.4 µg/m³ in 2009. From 2010 to 2014, the two PM_{2.5} indicators tended to decline, but the rate of decrease was almost negligible. In September 2013, the State Council of China promulgated its toughest-ever Air Pollution Prevention and Control Action Plan (APPCAP), and specific concentration goals were proposed for achievement by 2017 (The State Council of the People's Republic of China, 2013). In support of this plan, a series of stringent clean air measures were implemented, which included improving industrial and vehicle emission standards, phasing out small and polluting factories and power plants, upgrading industrial boilers, and promoting clean fuels in the residential sector (Zhang et al., 2019). The results of this study indicate that these measures effectively mitigated air pollution in China. The two PM_{2.5} indicators have declined dramatically since 2014, with the PW PM_{2.5} concentration decreasing by 15% (from 40.2 µg/m³ in 2014 to 34.0 µg/m³ in 2018). The interannual variation of the PM_{2.5} concentration in Japan did not fluctuate nearly as much. Japan's annual average PM_{2.5} concentration ranged from 10.5 to 16.1 µg/m³ and peaked in 2003; its annual PW PM_{2.5} concentration ranged from 12.6 µg/m³ to 17.8 µg/m³ (Fig. 2b). Because the Korean Peninsula is highly affected by long-range transport from China and Siberia, its annual PM_{2.5} concentration had a multimodal distribution, peaking in 1997, 2003, 2009, and 2014 (Fig. 2c). The long-term PW PM_{2.5} concentration

of Korean Peninsula was 20.9 µg/m³.

3.2. Trend and geographic distribution analyses

3.2.1. Time series trend analysis

The PM_{2.5} concentration in EA had an overall increasing trend from 1990 to 2019. However, the trend was very heterogeneous both spatially and temporally. To quantify the trend, the 30-year period was divided into three sub-periods: 1990–1999, 2000–2009, and 2010–2019. From 1990 to 1999, the trend was significant ($p < 0.05$) in south China and Korean Peninsula, and the regional rates of increase of PW PM_{2.5} concentrations were 0.3 µg/m³/yr and 0.4 µg/m³/yr, respectively. In terms of the spatial distribution, the significant increasing trend was found only in South Korea, whereas the trend in North Korea was not significant (Fig. 3a). Fig. S-8 in the supplementary material shows that although affected by the Asian financial crisis anthropogenic CO₂ emission in Korea dropped dramatically in 1998, it still kept a rapid growing trend in the 1990s. With this rapid growth, South Korea itself became a major source of PM_{2.5} pollution within the country, with emissions originating mainly from the traffic, construction, heating, and power generation sectors. This same process also occurred in the Pearl River Delta (PRD) region of south China, which is an important economic hub and a pioneer region for Chinese free-market reforms (Bickenbach and Liu, 2010; Chan, 2013). Since the 1980s, PRD has achieved rapid economic growth and has been regarded as the fastest growing area in China. The development of PRD attracted large inflows of labor from inland regions, and the population growth rate was particularly high between 1985 and 2000 (Oizumi, 2011). The rapid urbanization and industrialization boosted anthropogenic emissions, and the increase in the PM_{2.5} concentration in and around the PRD region was significant and much faster than in other areas (Fig. 3a). During the same time period, no significant trend was discovered in the northern part of China. Meanwhile, the result from EDGAR inventory revealed that before 2000 anthropogenic CO₂ emission in south China is higher than in east China (Fig. S-8b).

In 2000–2009, the PW PM_{2.5} concentrations in all regions increased substantially, except Japan (Table 2). Unlike other regions, anthropogenic CO₂ emission in Japan did not present any increase trend over the past decades and the nationwide emission always fluctuated around 1.0×10^9 ton/year (Fig. S-8a). As the Japanese government had already

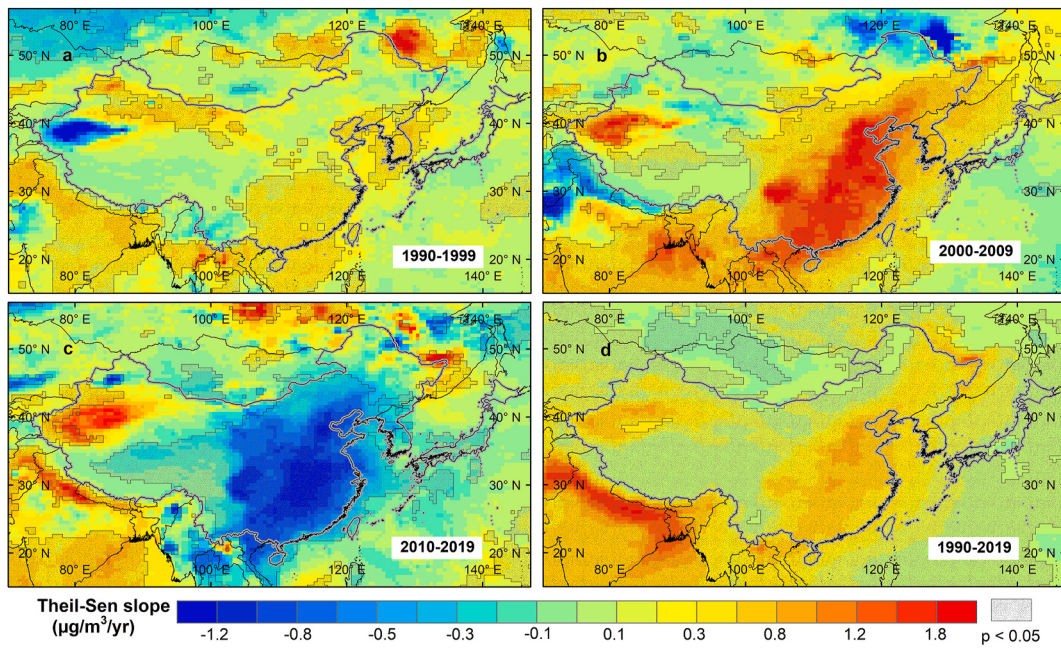


Fig. 3. Theil-Sen median trend of $\text{PM}_{2.5}$ concentration from 1990 to 2019: (a) 1990–1999, (b) 2000–2009, (c) 2010–2019, and (d) 1990–2019. The mesh indicates areas where $p < 0.05$.

Table 2
Theil-Sen median trend in the study region (unit: $\mu\text{g}/\text{m}^3/\text{yr}$).

Region	1990–1999		2000–2009		2010–2019		1990–2019		
	PM	PW $\text{PM}_{2.5}$	PM	PW $\text{PM}_{2.5}$	PM	PW $\text{PM}_{2.5}$	PM	PW $\text{PM}_{2.5}$	
China	East	0.1 (0.0–0.3)	0.2 (0.0–0.3)	1.3*** (1.0–1.6)	1.6*** (1.1–1.9)	-0.9*** (-1.1 to -0.6)	-0.9*** (-1.2 to -0.6)	0.6*** (0.4–0.6)	0.7*** (0.4–0.7)
	South	0.2** (0.1–0.3)	0.3** (0.1–0.3)	1.1*** (1.0–1.3)	1.4*** (1.1–1.6)	-0.7*** (-0.8 to -0.5)	-0.8*** (-1.0 to -0.6)	0.4*** (0.3–0.4)	0.5*** (0.4–0.5)
	North	0.1 (0.0–0.5)	0.1	0.3 (-0.2–0.8) (-0.1–0.5)	0.7** (0.3–1.0)	-0.2* (-0.3–0.0)	-0.4** (-0.5 to -0.1)	0.2*** (0.1–0.2)	0.3*** (0.2–0.3)
	West	0.0 (-0.4–0.4)	0.1 (-0.4–0.4)	0.2* (0.1–0.4) (-0.4–0.4)	0.4** (0.2–0.6)	0.1 (-0.2–0.4)	0.4 (-0.2–0.6)	0.2*** (0.1–0.2)	0.3*** (0.3–0.4)
	Nationwide	0.1 (0.0–0.4)	0.2* (0.0–0.3)	0.6*** (0.4–0.7)	1.3*** (1.0–1.5)	-0.2*** (-0.4 to -0.2)	-0.7*** (-1.0 to -0.6)	0.3*** (0.2–0.3)	0.5*** (0.4–0.6)
Japan			0.0 (-0.1–0.2)	0.1 (-0.1–0.2)	0.1* (0.0–0.2)	0.0 (-0.1–0.1)	-0.1 (-0.1–0.0)	-0.1 (-0.2–0.0)	0.1** (0.0–0.1)
	Korean Peninsula	0.3* (0.1–0.6)	0.4* (0.1–0.6)	0.6*** (0.5–0.7)	0.6*** (0.5–0.7)	-0.2 (-0.5–0.0)	-0.2 (-0.5–0.0)	0.2*** (0.2–0.3)	0.3*** (0.2–0.3)

Note: Data in parentheses refer to 95% confidence intervals. *, **, and *** indicate $p < 0.05$, $p < 0.01$ and $p < 0.001$, respectively.

pledged to the world to cut emissions 80% by 2050 and set a target of achieving a “decarbonized society”, the nationwide anthropogenic CO_2 emission even consecutively declined since 2013. By contrast, Table 2 indicates the increase of PW $\text{PM}_{2.5}$ concentrations in 2000–2009 was particularly high in east and south China (1.6 and $1.4 \mu\text{g}/\text{m}^3/\text{yr}$, respectively). Since the new century, China's economic development continued at a high rate and simultaneously annual anthropogenic CO_2 emission soared from 3.8×10^9 ton in 2000 to 1.1×10^{10} ton in 2018. Fig. S-8b reveal that the increase of anthropogenic CO_2 emission is more dramatic in the fast-developing south and east China and after 2000 anthropogenic CO_2 emission in east China gradually overtook south China and the gap between these two regions is still enlarging. As the emission from fossil fuel combustion makes a great contribution to forming primary and secondary $\text{PM}_{2.5}$, the increase of $\text{PM}_{2.5}$ concentration over 2000–2009 is much faster in east China. In terms of the spatial distribution, Fig. 3 show that $\text{PM}_{2.5}$ pollution worsened remarkably in the North China Plain, Yangtze Plain, PRD region, and Sichuan Basin, with rates exceeding $2 \mu\text{g}/\text{m}^3/\text{yr}$ from 2000 to 2009. Moreover, the increase was also faster and significant in the western part

of the Tarim Basin, but this change has been attributed primarily to interannual variation of DS aerosols rather than anthropogenic aerosols. Tables S-2 and Fig. S-3 also indicated that anthropogenic emission in west China (particularly in Tarim Basin, Tibetan Plateau) is extremely limited and the average annual anthropogenic CO_2 emission from 1997 to 2015 is 1.6×10^8 ton, much lower than other regions.

From 2010 to 2019, PW $\text{PM}_{2.5}$ concentrations significantly decreased in east, south, and north China (Table 2), with the greatest rate of decline in east China ($-0.9 \mu\text{g}/\text{m}^3/\text{yr}$). The declining tendency accelerated after 2014, and the decrease in PW $\text{PM}_{2.5}$ concentration in east China reached $-1.4 \mu\text{g}/\text{m}^3/\text{yr}$ from 2015 to 2019. Before 2010, China's air pollution control measures focused on SO_2 emitted from coal combustion to solve the acid rain problem. $\text{PM}_{2.5}$ was included as a criterion pollutant in the 2012 amendment of China's National Ambient Air Quality Standards, and the ambient $\text{PM}_{2.5}$ concentration had become the most important indicator of air pollution for urban residents in China. The result from EDGAR reveals that although anthropogenic CO_2 emission still keep an increase trend after 2011, the anthropogenic primary $\text{PM}_{2.5}$ emission has started to decline in EA (Fig. S-9). Unlike

previous policies, the formulation of APPCAP in 2013 was directly promoted by the State Council for the first time in the area of air pollution control and reflected China's determination to fight against PM_{2.5} pollution. APPCAP appears to have effectively reduced PM_{2.5} concentrations in China (Fig. 3c), particularly in the densely populated east and south parts. PM_{2.5} pollution mitigation activities in China are likely to influence air quality in neighboring countries. There were, in fact, decreases in Korean Peninsula and Japan, although they were not significant (Table 2).

3.2.2. Geographic distribution analysis

The SDEs, which delineate the overall characteristics of geospatial distributions, indicated that the main contributor to regional PM_{2.5} concentrations across the entire study area was China. There were high PM_{2.5} concentrations in both the eastern and western parts of China, although the dominant sources in these areas are from anthropogenic aerosols and natural aerosols, respectively. Fig. S-10 shows that the SDE of natural aerosols (DS and SS) extended along northwest of the study region and MEC mainly concentrated in Xinjiang Uygur Autonomous Region, while SDE of anthropogenic aerosols (BC, OC and SO₄) extended along south and east China and MEC distributed in Henan Province. The high PM_{2.5} concentrations in east and west of the study region resulted in a large SDE extending from west of the Xinjiang to the Yellow Sea. The MEC was located in eastern Gansu Province in the first sub-period (1990–1994) (Fig. 4). As anthropogenic emission gradually increased in the eastern part of China and the concentration of natural aerosols declined in western China (Fig. S-10), the MEC of PM_{2.5} began to shift eastward. Since 2000, increases of the PM_{2.5} concentrations in the eastern part of China substantially accelerated, and the MEC greatly shifted eastward in the third (2000–2004) and fourth sub-periods (2005–2009). Because the PM_{2.5} increase from 2000 to 2009 was greater in east and south China as compared to north part (Fig. 3b), the SDE rotated clockwise. The MEC reached its southeasternmost point (35.7 °N, 106.8 °E) in the fourth sub-period. After 2010, the MEC of PM_{2.5} moved northwest, and the SDE rotated counterclockwise. The MEC shift was more pronounced in the sixth sub-period (2015–2019) after implementation of APPCAP. The geographic distribution analysis of natural and anthropogenic aerosols revealed this variation is caused by two reasons. Firstly, the implementation of mitigation policies after 2010 substantially lowered PM_{2.5} concentrations in east and south China; secondly, natural emission of DS simultaneously enhanced in west China. Hence, both the MEC of natural and anthropogenic aerosols shifted westward after 2010 (Fig. S-10). Fig. S-11 presents the spatial distribution of the 5-year averages of PM_{2.5} concentrations over the

entire study area, and Tables S-3 presents the attributes of the SDEs and MECs.

3.3. Interannual variation of population exposed to PM_{2.5}

3.3.1. Regional population exposed to five pollution levels

In 2005, the WHO updated its AQG to offer appropriate targets for a broad range of policy options for worldwide air quality management (World Health Organization, 2005). The updated AQG and interim targets for annual PM_{2.5} concentrations are as follows: AQG, 10 µg/m³; interim target-3 (IT-3), 15 µg/m³; interim target-2 (IT-2), 25 µg/m³; and interim target-1 (IT-1), 35 µg/m³. In this study, the AQG and three interim targets were used as the break values to divide annual PM_{2.5} concentrations into five levels: Level 1 (PM_{2.5} concentration <10 µg/m³), Level 2 (10 µg/m³–<15 µg/m³), Level 3 (15 µg/m³ –<25 µg/m³), Level 4 (25 µg/m³ –<35 µg/m³), and Level 5 (PM_{2.5} concentration ≥35 µg/m³).

During 1990–2019, most of the Chinese population was exposed to Level 4 and Level 5 p.m._{2.5} concentrations (Fig. 5a), and only a total of 5.6% of the population was exposed to Level 1 and Level 2 pollution. Before 2000, Level 4 pollution was dominant in China, and 40.0% of the total population was exposed to it. Meanwhile, the annual population living in Level 5 was 170 million, or 13.8% of the Chinese population. As air quality gradually deteriorated in fast-growing regions, the population living at Level 5 dramatically increased, reaching 930 million in 2007 (Fig. S-12a) and accounting for 68.9% of the total population. At the same time, the proportion of the population exposed to Level 4 decreased to only 17.0%, its lowest point throughout the study period. As noted previously, the Chinese government implemented various measures to mitigate indigenous PM_{2.5} pollution after 2010. Fig. S-12a indicates that these measures have effectively decreased citizens' health risks through PM_{2.5} exposure, and the population affected by Level 5 pollution declined substantially to 600 million, or 41.7% of the total population, in 2018. Although air quality continued to improve in Chinese mega cities (e.g., Beijing and Shanghai) through 2019, ground-measured data indicated that PM_{2.5} levels in the rest of the country increased, particularly in south China, as industrial output and fossil fuel consumption kept climbing (Centre for Research on Energy and Clean Air, 2019). Consequently, Fig. S-12a shows that the population exposed to Level 5 increased to 720 million (over 50% of the population) by 2019. The population exposed to PM_{2.5} pollution has distinctive patterns in China's four subregions (Fig. S-13). The majority of the populations in east and south China were exposed to Level 4 and Level 5 pollution, and there was notable annual variation, most likely as a result of varying

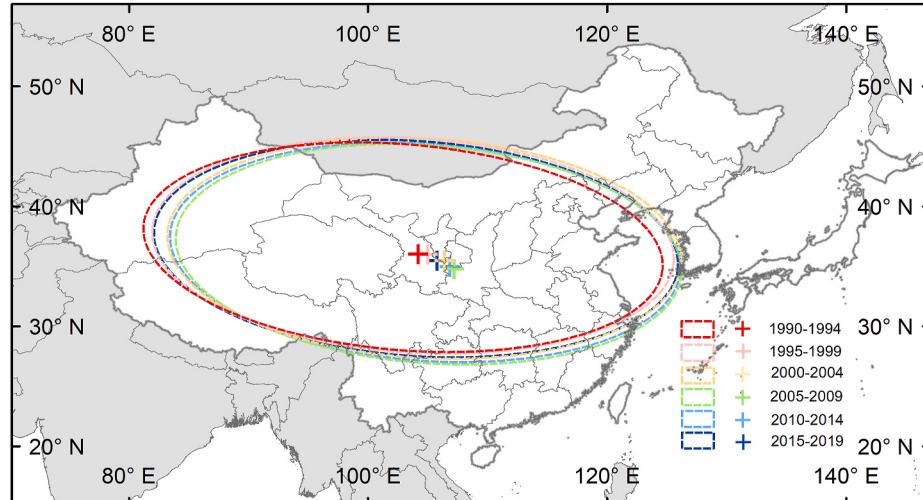


Fig. 4. Spatial variations in the MEC and SDE of the PM_{2.5} concentrations over EA from 1990 to 2019.

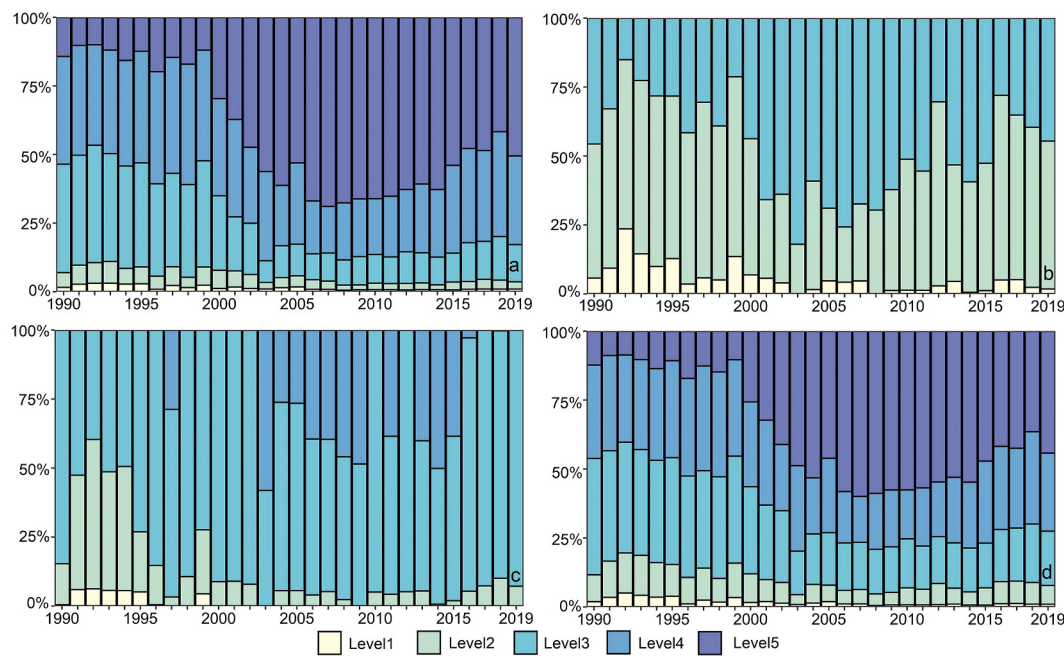


Fig. 5. Percent of the population exposed to different PM_{2.5} concentration levels from 1990 to 2019: (a) China, (b) Japan, (c) Korean Peninsula, and (d) EA. Annual PM_{2.5} concentration was divided into five levels: Level 1 (PM_{2.5} concentration <10 µg/m³), Level 2 (10 µg/m³–<15 µg/m³), Level 3 (15 µg/m³–<25 µg/m³), Level 4 (25 µg/m³–<35 µg/m³), and Level 5 (\geq 35 µg/m³).

anthropogenic emissions and changing emission control policies. Level 3 pollution dominated in north China, and its annual variation pattern has also been greatly influenced by anthropogenic factors. By contrast, the proportion of the population exposed to the five pollution levels was stable in west China, and there was no significant interannual variation from 1990 to 2019. Refer to Fig. S-13 in the supplementary material for detailed information on the four subregions of China.

Japan is the only country in EA to have a declining population since 2009 (Fig. S-12b). Its population also has lower health risks as a result of PM_{2.5} exposure than those of China and Korean Peninsula. Before 2000, approximately 60% of the population was exposed to Level 2 pollution, and this declined to only 18.0% in 2003. This exposure was probably related to long-range transported particles from several large boreal forest fires in Siberia at that time. From 2001 to 2010, the population living at Level 3 was consistently high, accounting for two-thirds of the nationwide population. Since 2015, this gradually decreased to about 30%.

Throughout the study period, most of the population of Korean Peninsula was exposed to Level 3 pollution, and before 2001, almost no one experienced Level 4 pollution, except in 1997. Because of an increase in indigenous pollution and the long-range transport of pollutants from China or other regions, the percentage of the population exposed to Level 4 substantially increased from 2002 to 2015. As in Japan, the population exposed to Level 4 soared to 58.1% in 2003 at the time of the Siberian forest fires. Since 2014, the percentage of the Korean population living at Level 4 substantially declined, dropping to nearly zero in 2017, 2018, and 2019. This trend is consistent with the observed variations of the population exposed to Level 5 in China.

3.3.2. Health risk of population and age groups exposed to PM_{2.5}

Besides PM_{2.5} concentration, population size is also an important factor to evaluate the health impact of PM_{2.5} exposure. Meanwhile, China is experiencing rapid urbanization in the past decades and massive west and north rural and sub-urban population moved to southeast mega-cities. Particularly, population loss in northeast China has become increasingly severe and has drawn considerable attention from domestic and international researchers, as well as the Chinese

government (Simini et al., 2012; Zhu et al., 2020; You et al., 2021). Thus, in this section population densities were multiplied by PM_{2.5} concentrations to evaluate the health risk in EA. Comparing with the geographic distribution analysis of PM_{2.5} (Fig. 4), SDE and MEC of health risk presented different spatial pattern. As a result of the high population density and severe PM_{2.5} pollution in east and south China, the SDE of health risk is much smaller and MEC mainly concentrated in Henan province (Fig. S-14). Although, the PM_{2.5} pollution in east and south China significantly mitigated since 2010, Fig. S-14 and Tables S-4 shows that the MEC of health risk did not shift westward, and it even slightly moved east in the fifth (2009–2014) and sixth sub-periods (2015–2019). The geographic distribution analysis of population density indicated that this is likely to be caused by the population flow from north and west China to southeast China. The MEC of population density presented a trend of moving southeast and SDE also rotated clockwise from 1990 to 2019 (Fig. S-14 and Tables S-5). It implies that although the emission control policies and measures effectively declined PM_{2.5} concentration of east and south China, the inherent huge population and continuing population inflow caused that the regional health risk related to PM_{2.5} exposure did not effectively relieve since 2010.

The cumulative percentage of the exposed population was also calculated. As can be seen in Fig. 6b, the population/exposure curves did not change noticeably from 1990 to 1999, and the population exposed to heavy PM_{2.5} pollution was extremely small (<1% exposed to PM_{2.5} > 50 µg/m³). After 1999, the curves started to shift to the right as the population exposed to serious PM_{2.5} pollution increased dramatically. Then, the proportion of population exposed to PM_{2.5} > 50 µg/m³ soared from 1.0% in 2001 to 25.0% in 2008–2009. Since 2013 and the implementation of APPCAP, air quality in China gradually improved, and consequently, the curves greatly shifted leftward. In 2018, 2019, the population exposed to PM_{2.5} below Level 4 returned to 59.4%, and the proportion exposed to PM_{2.5} > 50 µg/m³ dropped to 6.2%.

Because older adults are the most susceptible population to cardiovascular and respiratory diseases, ambient PM_{2.5} pollution has the greatest potential to affect their health (Wang et al., 2015; Goto et al., 2016). EA is experiencing the issue of population aging to an unprecedented degree. Older adults (age \geq 65) increased from 6.2% of the total

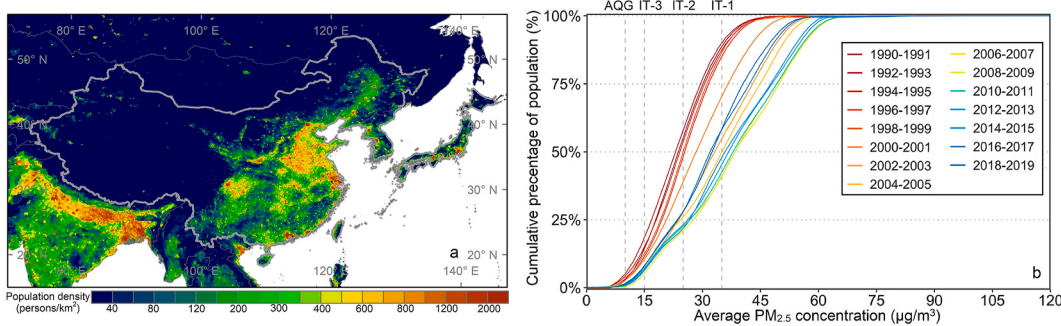


Fig. 6. Average population density (left panel) and proportion of the population exposed to different PM_{2.5} concentrations from 1990 to 2019 (right panel).

population in 1990 to 12.8% in 2019 (Fig. 7a and b; United Nations, 2019). The total population of EA rose from 1.36 billion to 1.64 billion during the same time period, and the net increase of older adults was 126 million.

The population of older adults exposed to Level 5 pollution was approximately 10 million from 1990 to 1999, whereas it was only seven million in 1991 and 1992. Since 2000, the worsening PM_{2.5} pollution in China combined with the increasing aging population caused a dramatic increase in the number of older adults living at Level 5; the number increased almost eightfold to 78.7 million by 2014. Moreover, the older adult population living at Level 5 grew much faster than the other age groups (Fig. 7c). With the introduction of air pollution mitigation measures in China, the older adult population living at Level 5 decreased to 65.0 million in 2018. China's increased coal consumption caused regional PM_{2.5} pollution to deteriorate again in 2019 (Friedlingstein et al., 2019; Centre for Research on Energy and Clean Air, 2019). Although the pollution level in 2019 was less than it was in the heavily polluted years (2005–2014), the corresponding older adult population exposed to Level 5 rose to 83.1 million, the highest in the study period (Fig. 7c). This implies that, as the population aging further intensifies in the upcoming decades, EA will face more serious challenges in air quality management, and more efforts will be required to reduce anthropogenic emissions of primary PM_{2.5} and its precursors.

3.4. Comparison with ground-measurement and uncertainties of MERRA-2 estimated PM_{2.5}

MERRA-2 estimated PM_{2.5} concentrations were compared with ground-measurement data. The annual PM_{2.5} concentrations of 49 Japanese cities, seven Korean cities, and 363 Chinese cities were obtained from Japan's Ministry of the Environment, the Korean Statistical Information Service, and China's National Environmental Monitoring Center. Because China had no effective PM_{2.5} monitoring network before 2015, the temporal coverage of the collected ground data is from 2015 to 2018. The locations of the 419 cities are shown in Fig. 8. The linear regression of PM_{2.5} concentrations estimated by MERRA-2 against

ground-observed PM_{2.5} had a correlation coefficient of 0.83. Moreover, the World Air Quality Report of IQAir calculated the PW PM_{2.5} concentration from ground-based monitoring stations and available city data and revealed that China's city-level PW PM_{2.5} concentration (excluding rural regions) was 39.1 µg/m³ in 2019 (IQAir, 2019). The corresponding concentration from MERRA-2 (including rural regions) was 35.6 ± 4.7 µg/m³ (Fig. 2a), which is consistent with the World Air Quality Report value. However, Fig. 8 also shows that the values estimated by MERRA-2 were lower overall than the ground measurements, possibly for two main reasons. First, most of the PM_{2.5} monitoring stations are located in high-traffic urban areas, where the corresponding PM_{2.5} concentrations are much higher than in other areas. Second, the spatial resolution of MERRA-2 is 0.5° × 0.625°, and the estimated values represent the average PM_{2.5} concentration of a vast region, whereas ground-measured data represent only the actual conditions around the monitoring stations. Therefore, we assumed that PM_{2.5} concentrations estimated by MERRA-2 were likely to underestimate urban PM_{2.5} pollution. In addition, differences in instruments, monitoring methods, and station sites (e.g., elevation, vegetation, and wind conditions) can also affect the comparability of these measurements.

Fig. S-15 and Tables S-6 indicate that bias between MERRA-estimated PM_{2.5} concentration and ground-measurement data in study region presented strong spatial pattern. MERRA-estimated PM_{2.5} concentration in south China, Korea and Japan is much closer to ground-measurement data. The average root mean square error (RMSE) in these three regions are 7.7 ± 1.3 µg/m³, 3.7 ± 1.2 µg/m³, and 3.2 ± 0.6 µg/m³, respectively, which is much lower than in other regions. Although, the average RMSE of 120 cities in east China is 16.6 ± 1.6 µg/m³ and the high RMSE mainly distributed in the cities of heavily polluted North China Plain, the average normalized RMSE (NRMSE) of east China is relatively lower and the value is 28 ± 5% that is close to the average NRMSE in south China. In contrast, both RMSE and NRMSE reveal that these are high bias between MERRA-estimated PM_{2.5} concentration and ground-measurement data in north and west China, particularly in Tibetan Plateau. Tables S-6 shows that the average RMSE and NRMSE in north and west China exceeded 15 µg/m³ and 40%,

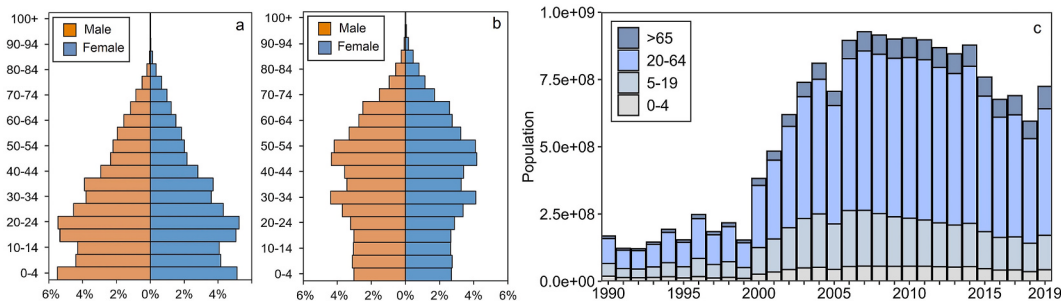


Fig. 7. (a) The population pyramid of EA in (a) 1990 and (b) 2019. (c) The population of different age groups exposed to Level 5 pollution (PM_{2.5} concentration $\geq 35 \mu\text{g}/\text{m}^3$).

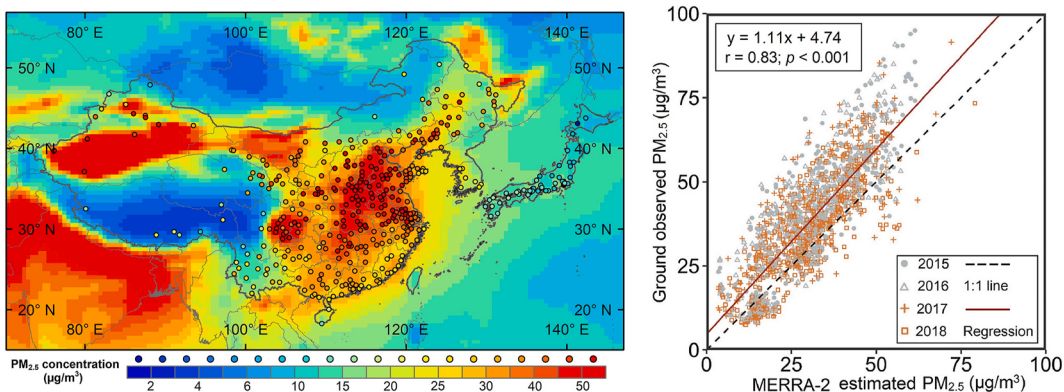


Fig. 8. Comparison of ground-measurement and MERRA-2 estimated PM_{2.5} (left panel) and the correlation between the two datasets (right panel).

separately. These two regions are both characterized by less populous, limited urban agglomeration and anthropogenic emission, and easily affected by natural emission. Therefore, the coarse resolution of MERRA-2 is more likely to fuse urban PM_{2.5} concentration with surroundings and omit spatial features of urban PM_{2.5} distribution in north and west China.

Aerosols in MERRA-2 are simulated with an online version of the Goddard Chemistry, Aerosol, Radiation, and Transport model (GOCART) and the bias corrected AOD is assimilated (Chin et al., 2002). Aerosol and precursor emissions of the model are obtained from various inventory and satellite derived datasets like EDGAR and NASA Quick Fire Emission Dataset (QFED) (Buchard et al., 2015). The monthly emissions used in MERRA-2 are temporally interpolated by linear interpolation, which is possibly to enlarge the uncertainties of monthly aerosol concentration. Moreover, besides PM_{2.5} concentration, the monthly variation of AOD is affected by other factors, such as planetary boundary layer height, relative humidity, and it tends to present high value in summer. That is also likely to enlarge the uncertainties of monthly MERRA-2 products. Ma et al. (2020) compares the variations of monthly PM_{2.5} concentration between MERRA-estimated and ground-measurement in China. And they found MERRA-estimated PM_{2.5} shows the best agreements with observations in summer and the discrepancy significantly enlarged in winter. On a regional scale, MERRA-estimated PM_{2.5} concentration exhibits obvious monthly variation in Pearl River delta and Yangtze River Delta. While, the monthly variation in Beijing-Tianjin-Hebei region is much flatter and shows large discrepancy with observations.

The coarse resolution of MERRA-2 makes it applicable only to large-scale studies, such as those on continental and global scales. In small-scale studies or the region with less population and limited anthropogenic emission (e.g. north and west China), the coarse resolution may obscure and omit spatial features of PM_{2.5} distribution in urban area that could lead to large uncertainties. Meanwhile, if the analysis is conducted on a monthly or daily level instead of an annual level, it is essential to consider the strong seasonality of discrepancy between MERRA-estimated PM_{2.5} and ground-measurement and it is better to use different estimation equations for each season. The most essential advantage of MERRA-2 is that it can be used to estimate PM_{2.5} concentrations over several decades. It has a long temporal coverage, which is suitable for long time-series studies. Additionally, the amount of ground-observed and remote-sensing-retrieved PM_{2.5} concentration data have gradually increased after 2000, particularly after 2010, and the data before 2000 are very sparse. In contrast, MERRA-2 is able to estimate PM_{2.5} concentrations before 2000, which is vital to health studies globally or in heavily polluted regions. Overall, the long temporal coverage of MERRA-2 substantially compensates for the limitations imposed by its coarse resolution.

4. Conclusions

In this study, MERRA-2 data were used to estimate PM_{2.5} concentrations over EA, and spatiotemporal patterns and variations from 1990 to 2019 were analyzed. We also comprehensively examined trends in populations exposed to different PM_{2.5} pollution levels. The results indicated that the spatial distribution of five kinds of aerosols and PM_{2.5} are distinctive over EA. The anthropogenic aerosols (BC, OC, and SO₄) were at higher concentrations in the fast-growing and densely populated east and south China, whereas natural DS and SS aerosols were much higher in the arid west China and coastal areas. Because they are affected by long-range transport, interannual variations of PM_{2.5} concentrations in Japan and Korean Peninsula were closely related to anthropogenic emissions and the emission control policies in China. From 1990 to 1999, significant increases in PM_{2.5} were only observed in the southern part of China and in South Korea. During that period, 88% of EA's population lived below Level 4 (PM_{2.5} ≤ 35 µg/m³), and only a small part of the region's population experienced heavy PM_{2.5} pollution. Since 2000, increasing anthropogenic emissions stemming from China's economic growth contributed substantially to increased regional PM_{2.5} pollution. The rate of increase of PW PM_{2.5} concentrations increased dramatically, reaching 1.6 µg/m³/yr in east and 1.4 µg/m³/yr in south China in 2000–2009. At the same time, the proportion of the population exposed to low levels of PM_{2.5} pollution became increasingly smaller, and the proportion experiencing Level 5 pollution rose to approximate 50%.

As PM_{2.5} pollution in China began to draw worldwide attention, the central government of China attempted to implement some measures to mitigate nationwide PM_{2.5} pollution. However, these measures were not very effective, and the PM_{2.5} concentration did not significantly decline from 2010 to 2013. In 2013, the State Council of China directly promoted and promulgated APPCAP, and that series of clean air measures effectively decreased PM_{2.5} pollution in China, particularly in the heavily polluted east and south China. As air quality improved, the population exposed to a PM_{2.5} concentration below Level 4 grew to 63.5% in 2018. The age-group analysis indicated that the older adult population exposed to Level 5 pollution peaked at 83.1 million in 2019. Because the issue of population aging is becoming more and more serious in EA, strict control of the emission of primary PM_{2.5} and its precursors is required to reduce the potential health risk faced by residents of the regions.

CRediT authorship contribution statement

Shuai Yin: Conceptualization, Methodology, Software, Visualization, Validation, Writing – original draft, Writing – review & editing.

Declaration of competing interest

We would like to submit the manuscript entitled “Decadal trends of MERRA-estimated PM_{2.5} concentrations in East Asia and potential exposure from 1990 to 2019”, which we wish to be considered for publication in “Atmospheric Environment”. No conflict of interest exists in the submission of this manuscript, and manuscript is approved by all authors for publication. I would like to declare on behalf of my co-authors that the work described was original research that has not been published previously, and not under consideration for publication elsewhere, in whole or in part. All the authors listed have approved the manuscript that is enclosed.

Acknowledgements

We are grateful to NASA’s Global Modeling and Assimilation Office and Socioeconomic Data and Applications Center, EDGAR and GFED for the use of their data. Without their hardworking, we cannot obtain sufficient data to support this study.

Appendix A. Supplementary data

Supplementary data to this article can be found online at <https://doi.org/10.1016/j.atmosenv.2021.118690>.

References

- Akagi, S.K., Yokelson, R.J., Wiedinmyer, C., Alvarado, M.J., Reid, J.S., Karl, T., Crouse, J.D., Wennberg, P.O., 2011. Emission factors for open and domestic biomass burning for use in atmospheric models. *Atmos. Chem. Phys.* 11 (9), 4039–4072.
- Benedetti, A., Morcrette, J.J., Boucher, O., Dethof, A., Engelen, R.J., Fisher, M., Plentje, H., Huneeus, N., Jones, L., Kaiser, J.W., Kinne, S., 2009. Aerosol analysis and forecast in the European centre for medium-range weather forecasts integrated forecast system: 2. Data assimilation. *J. Geophys. Res. Atmos.* 114 (D13).
- Bertschi, I.T., Jaffe, D.A., 2005. Long-range transport of ozone, carbon monoxide, and aerosols to the NE Pacific troposphere during the summer of 2003: observations of smoke plumes from Asian boreal fires. *J. Geophys. Res. Atmos.* 110 (D5).
- Bickenbach, F., Liu, W.H., 2010. On the role of personal relationships for doing business in the Greater Pearl River Delta, China. *China Econ. J.* 3 (3), 281–306.
- Brauer, M., Freedman, G., Frostad, J., Van Donkelaar, A., Martin, R.V., Dentener, F., Dingenen, R.V., Estep, K., Amini, H., Apte, J.S., Balakrishnan, K., 2016. Ambient air pollution exposure estimation for the global burden of disease 2013. *Environ. Sci. Technol.* 50 (1), 79–88.
- Buchard, V., Da Silva, A.M., Colarco, P.R., Darmenov, A., Randles, C.A., Govindaraju, R., Torres, O., Campbell, J., Spurr, R., 2015. Using the OM1 aerosol index and absorption aerosol optical depth to evaluate the NASA MERRA Aerosol Reanalysis. *Atmos. Chem. Phys.* 15 (10), 5743–5760.
- Buchard, V., Da Silva, A.M., Randles, C.A., Colarco, P., Ferrare, R., Hair, J., Hostetler, C., Tackett, J., Winker, D., 2016. Evaluation of the surface PM_{2.5} in version 1 of the NASA MERRA aerosol reanalysis over the United States. *Atmos. Environ.* 125, 100–111.
- Buchard, V., Randles, C.A., da Silva, A.M., Darmenov, A., Colarco, P.R., Govindaraju, R., Ferrare, R., Hair, J., Beyersdorf, A.J., Ziembka, L.D., Yu, H., 2017. The MERRA-2 aerosol reanalysis, 1980 onward. Part II: evaluation and case studies. *J. Clim.* 30 (17), 6851–6872.
- Centre for Research on Energy and Clean Air, 2019. Air Pollution in China 2019. <https://energyandcleanair.org/publications/china-winter-targets-2019-2020/>.
- Chen, C.K.C., 2013. Contesting class organization: migrant workers’ strikes in China’s Pearl River delta, 1978–2010. *Int. Labor Work. Class Hist.* 83, 112–136.
- Chen, L.W.A., Doddridge, B.G., Dickerson, R.R., Chow, J.C., Mueller, P.K., Quinn, J., Butler, W.A., 2001. Seasonal variations in elemental carbon aerosol, carbon monoxide and sulfur dioxide: implications for sources. *Geophys. Res. Lett.* 28 (9), 1711–1714.
- Chin, M., Ginoux, P., Kinne, S., Torres, O., Holben, B.N., Duncan, B.N., Martin, R.V., Logan, J.A., Higurashi, A., Nakajima, T., 2002. Tropospheric aerosol optical thickness from the GOCART model and comparisons with satellite and Sun photometer measurements. *J. Atmos. Sci.* 59 (3), 461–483.
- Chung, Y.S., 1992. On the observations of yellow sand (dust storms) in Korea. *Atmos. Environ.* 26 (15), 2743–2749.
- Cohen, A.J., Brauer, M., Burnett, R., Anderson, H.R., Frostad, J., Estep, K., Balakrishnan, K., Brunekreef, B., Dandona, L., Dandona, R., Feigin, V., 2017. Estimates and 25-year trends of the global burden of disease attributable to ambient air pollution: an analysis of data from the Global Burden of Diseases Study 2015. *Lancet* 389, 1907–1918.
- Cooke, W.F., Wilson, J.J., 1996. A global black carbon aerosol model. *J. Geophys. Res. Atmos.* 101 (D14), 19395–19409.
- Crippa, M., Guizzardi, D., Muntean, M., Schaaf, E., Dentener, F., van Aardenne, J.A., Monni, S., Doering, U., Olivier, J.G., Pagliari, V., Janssens-Maenhout, G., 2018. Gridded emissions of air pollutants for the period 1970–2012 within EDGAR v4.3.2. *Earth Syst. Sci. Data* 10 (4), 1987–2013.
- Crippa, M., Solazzo, E., Huang, G., Guizzardi, D., Koffi, E., Muntean, M., Schieberle, C., Friedrich, R., Janssens-Maenhout, G., 2020. High resolution temporal profiles in the emissions database for global atmospheric research. *Sci. Data* 7 (1), 1–17.
- Doxsey-Whitfield, E., MacManus, K., Adamo, S.B., Pistolesi, L., Squires, J., Borkovska, O., Baptista, S.R., 2015. Taking advantage of the improved availability of census data: a first look at the gridded population of the world, version 4. *Appl. Geogr.* 1 (3), 226–234.
- Friedlingstein, P., et al., 2019. Global carbon budget 2019. *Earth Syst. Sci. Data* 11 (4), 1783–1838.
- Ghude, S.D., Chate, D.M., Jena, C., Beig, G., Kumar, R., Barth, M.C., Pfister, G.G., Fadnavis, S., Pithani, P., 2016. Premature mortality in India due to PM_{2.5} and ozone exposure. *Geophys. Res. Lett.* 43 (9), 4650–4658.
- Giglio, L., Randerson, J.T., van der Werf, G.R., 2013. Analysis of daily, monthly, and annual burned area using the fourth-generation global fire emissions database (GFED4). *J. Geophys. Res. Biogeosci.* 118 (1), 317–328.
- Goldammer, J.G., 2001. Fire situation in Mongolia. *Int. For. Fire News* 26, 75–83.
- Goto, D., Ueda, K., Ng, C.F.S., Takami, A., Ariga, T., Matsuhashi, K., Nakajima, T., 2016. Estimation of excess mortality due to long-term exposure to PM_{2.5} in Japan using a high-resolution model for present and future scenarios. *Atmos. Environ.* 140, 320–332.
- Hallquist, M., Wenger, J.C., Baltensperger, U., Rudich, Y., Simpson, D., Claeys, M., Dommen, J., Donahue, N.M., George, C., Goldstein, A.H., Hamilton, J.F., 2009. The formation, properties and impact of secondary organic aerosol: current and emerging issues. *Atmos. Chem. Phys.* 9 (14), 5155–5236.
- Hoaglin, D.C., Mosteller, F., Tukey, J.W., 2000. Understanding Robust and Exploratory Data Analysis. Wiley & Sons, New York.
- Husar, R.B., Tratt, D.M., Schichtel, B.A., Falke, S.R., Li, F., Jaffe, D., Gasso, S., Gill, T., Lauhainen, N.S., Lu, F., Reheis, M.C., 2001. Asian dust events of April 1998. *J. Geophys. Res. Atmos.* 106 (D16), 18317–18330.
- Ikemori, F., Honjyo, K., Yamagami, M., Nakamura, T., 2015. Influence of contemporary carbon originating from the 2003 Siberian forest fire on organic carbon in PM_{2.5} in Nagoya, Japan. *Sci. Total Environ.* 530, 403–410.
- IPCC, 2007. Climate Change 2007: Mitigation of Climate Change. Working Group III Contribution to the Fourth Assessment Report of the Intergovernmental Panel on Climate Change. Cambridge University Press, Cambridge, UK and New York, USA.
- IQAir, 2019. World Air Quality Report 2019. Region & City PM_{2.5} Ranking. <https://www.iqair.com/world-most-polluted-cities/world-air-quality-report-2019-en.pdf>.
- Jaffe, D., Bertschi, I., Jaegli, L., Novelli, P., Reid, J.S., Tanimoto, H., Vingarzan, R., Westphal, D.L., 2004. Long-range transport of Siberian biomass burning emissions and impact on surface ozone in western North America. *Geophys. Res. Lett.* 31, L16106.
- Janssens-Maenhout, G., Crippa, M., Guizzardi, D., Muntean, M., Schaaf, E., Dentener, F., Bergamaschi, P., Pagliari, V., Olivier, J.G., Peters, J.A., van Aardenne, J.A., 2019. EDGAR v4.3.2 Global Atlas of the three major greenhouse gas emissions for the period 1970–2012. *Earth Syst. Sci. Data* 11 (3), 959–1002.
- Jeong, J.I., Park, R.J., Youn, D., 2008. Effects of Siberian forest fires on air quality in East Asia during May 2003 and its climate implication. *Atmos. Environ.* 42 (39), 8910–8922.
- Kaneyasu, N., Igarashi, Y., Sawa, Y., Takahashi, H., Takada, H., Kumata, H., Hoeller, R., 2007. Chemical and optical properties of 2003 Siberian forest fire smoke observed at the summit of Mt. Fuji, Japan. *J. Geophys. Res. Atmos.* 112 (D13).
- Kaneyasu, N., Yamamoto, S., Sato, K., Takami, A., Hayashi, M., Hara, K., Kawamoto, K., Okuda, T., Hatakeyama, S., 2014. Impact of long-range transport of aerosols on the PM_{2.5} composition at a major metropolitan area in the northern Kyushu area of Japan. *Atmos. Environ.* 97, 416–425.
- Laden, F., Neas, L.M., Dockery, D.W., Schwartz, J., 2000. Association of fine particulate matter from different sources with daily mortality in six US cities. *Environ. Health Perspect.* 108 (10), 941–947.
- Lee, K.H., Kim, J.E., Kim, Y.J., Kim, J., von Hoyningen-Huene, W., 2005. Impact of the smoke aerosol from Russian forest fires on the atmospheric environment over Korea during May 2003. *Atmos. Environ.* 39 (1), 85–99.
- Lee, S., Ho, C.H., Lee, Y.G., Choi, H.J., Song, C.K., 2013. Influence of transboundary air pollutants from China on the high-PM₁₀ episode in Seoul, Korea for the period October 16–20, 2008. *Atmos. Environ.* 77, 430–439.
- Lefever, D.W., 1926. Measuring geographic concentration by means of the standard deviational ellipse. *Am. J. Sociol.* 32 (1), 88–94.
- Li, T.C., Yuan, C.S., Huang, H.C., Lee, C.L., Wu, S.P., Tong, C., 2017. Clustered long-range transport routes and potential sources of PM_{2.5} and their chemical characteristics around the Taiwan Strait. *Atmos. Environ.* 148, 152–166.
- Liousse, C., Penner, J.E., Chuang, C., Walton, J.J., Eddleman, H., Cachier, H., 1996. A global three-dimensional model study of carbonaceous aerosols. *J. Geophys. Res. Atmos.* 101 (D14), 19411–19432.
- Liu, Y., Park, R.J., Jacob, D.J., Li, Q., Kilaru, V., Sarnat, J.A., 2004. Mapping annual mean ground-level PM_{2.5} concentrations using Multiangle Imaging Spectroradiometer aerosol optical thickness over the contiguous United States. *J. Geophys. Res. Atmos.* 109 (D22).
- Lu, F., Xu, D., Cheng, Y., Dong, S., Guo, C., Jiang, X., Zheng, X., 2015. Systematic review and meta-analysis of the adverse health effects of ambient PM_{2.5} and PM₁₀ pollution in the Chinese population. *Environ. Res.* 136, 196–204.
- Ma, J., Xu, J., Qu, Y., 2020. Evaluation on the surface PM_{2.5} concentration over China mainland from NASA’s MERRA-2. *Atmos. Environ.* 237, 117666.

- Maji, K.J., Dikshit, A.K., Arora, M., Deshpande, A., 2018. Estimating premature mortality attributable to PM_{2.5} exposure and benefit of air pollution control policies in China for 2020. *Sci. Total Environ.* 612, 683–693.
- McCarty, W., Coy, L., Gelaro, R., Huang, A., Merkova, D., Smith, E.B., Sienkiewicz, M., Wargan, K., 2016. MERRA-2 Input Observations: Summary and Assessment. NASA Tech. Rep. Series on Global Modeling and Data Assimilation, NASA/TM-2016-104606, vol. 46, p. 64.
- Munir, S., Habeebulah, T.M., Seroji, A.R., Gabr, S.S., Mohammed, A.M., Morsy, E.A., 2013. Quantifying temporal trends of atmospheric pollutants in Makkah (1997–2012). *Atmos. Environ.* 77, 647–655.
- Murayama, T., Müller, D., Wada, K., Shimizu, A., Sekiguchi, M., Tsukamoto, T., 2004. Characterization of Asian dust and Siberian smoke with multi-wavelength Raman lidar over Tokyo, Japan in spring 2003. *Geophys. Res. Lett.* 31, L23103.
- Oh, H.R., Ho, C.H., Kim, J., Chen, D., Lee, S., Choi, Y.S., Chang, L.S., Song, C.K., 2015. Long-range transport of air pollutants originating in China: a possible major cause of multi-day high-PM10 episodes during cold season in Seoul, Korea. *Atmos. Environ.* 109, 23–30.
- Oizumi, K., 2011. The emergence of the Pearl River delta economic zone: challenges on the path to megaregion status and sustainable growth. *Pac. Bus. Ind.* 11 (41), 2–20.
- Onishi, K., Kuroasaki, Y., Otani, S., Yoshida, A., Sugimoto, N., Kurozawa, Y., 2012. Atmospheric transport route determines components of Asian dust and health effects in Japan. *Atmos. Environ.* 49, 94–102.
- Randerson, J.T., Chen, Y., van der Werf, G.R., Rogers, B.M., Morton, D.C., 2012. Global burned area and biomass burning emissions from small fires. *J. Geophys. Res. Biogeosci.* 117 (G4).
- Randles, C.A., da Silva, A.M., Buchard, V., Colarco, P.R., Darmenov, A., Govindaraju, R., Smirnov, A., Holben, B., Ferrare, R., Hair, J., Shinozuka, Y., 2017. The MERRA-2 aerosol reanalysis, 1980 onward. Part I: system description and data assimilation evaluation. *J. Clim.* 30 (17), 6823–6850.
- Rienecker, M.M., Suarez, M.J., Gelaro, R., Todling, R., Bacmeister, J., Liu, E., Bosilovich, M.G., Schuber, S.D., Takacs, L., Kim, G.-K., Bloom, S., Chen, J., Collins, D., Conaty, A., da Silva, A., Gu, W., Joiner, J., Koster, R.D., Lucchesi, R., Molod, A., Owens, T., Pawson, S., Pegion, P., Redder, C.R., Reichle, R., Robertson, F.R., Ruddick, A.G., Sienkiewicz, M., Woollen, J., 2011. MERRA: NASA's modern-era retrospective analysis for research and applications. *J. Clim.* 24 (14), 3624–3648.
- Sekiya, T.T., Tanaka, T.Y., Shimizu, A., Miyoshi, T., 2010. Data assimilation of CALIPSO aerosol observations. *Atmos. Chem. Phys.* 10, 39–49.
- Sen, P.K., 1968. Estimates of the regression coefficient based on Kendall's tau. *J. Am. Stat. Assoc.* 63, 1379–1389.
- Shao, P., Xin, J., An, J., Kong, L., Wang, B., Wang, J., Wang, Y., Wu, D., 2017. The empirical relationship between PM_{2.5} and AOD in nanjing of the Yangtze River delta. *Atmos. Pollut. Res.* 8 (2), 233–243.
- Simini, F., González, M.C., Maritan, A., Barabási, A., 2012. A universal model for mobility and migration patterns. *Nature* 484 (7392), 96–100.
- Song, W., Jia, H., Huang, J., Zhang, Y., 2014. A satellite-based geographically weighted regression model for regional PM_{2.5} estimation over the Pearl River Delta region in China. *Remote Sens. Environ.* 154, 1–7.
- Stieb, D.M., Chen, L., Beckerman, B.S., Jerrett, M., Crouse, D.L., Omariba, D.W., Peters, P.A., van Donkelaar, A., Martin, R.V., Burnett, R.T., Gilbert, N.L., 2016. Associations of pregnancy outcomes and PM in a national Canadian study. *Environ. Health Perspect.* 124, 243–249.
- Theil, H., 1950. A rank invariant method of linear and polynomial regression analysis, part 3. *Proc. Koninklijke Nederlandse Akademie Wetenschappen A* 53, 1397–1412.
- The State Council of the People's Republic of China, 2013. Air Pollution Prevention and Control Action Plan. http://www.gov.cn/zwgk/2013-09/12/content_2486773.htm.
- Turpin, B.J., Saxena, P., Andrews, E., 2000. Measuring and simulating particulate organics in the atmosphere: problems and prospects. *Atmos. Environ.* 34 (18), 2983–3013.
- United Nations, 2019. World Population Prospects 2019: Highlights. Department of Economic and Social Affairs, Population Division.
- van der Werf, G.R., Randerson, J.T., Giglio, L., Collatz, G.J., Mu, M., Kasibhatla, P.S., Morton, D.C., DeFries, R.S., Jin, Y.V., van Leeuwen, T.T., 2010. Global fire emissions and the contribution of deforestation, savanna, forest, agricultural, and peat fires (1997–2009). *Atmos. Chem. Phys.* 10 (23), 11707–11735.
- van der Werf, G.R., Randerson, J.T., Giglio, L., van Leeuwen, T.T., Chen, Y., Rogers, B.M., Mu, M., van Marle, M.J., Morton, D.C., Collatz, G.J., Yokelson, R.J., 2017. Global fire emissions estimates during 1997–2016. *Earth Syst. Sci. Data* 9 (2), 697–720.
- Vanem, E., Walker, S.E., 2013. Identifying trends in the ocean wave climate by time series analyses of significant wave height data. *Ocean Eng.* 61, 148–160.
- Wang, C., Tu, Y., Yu, Z., Lu, R., 2015. PM_{2.5} and cardiovascular diseases in the elderly: an overview. *Int. J. Environ. Res. Publ. Health* 12 (7), 8187–8197.
- Wang, J., Christopher, S.A., 2003. Intercomparison between satellite-derived aerosol optical thickness and PM_{2.5} mass: implications for air quality studies. *Geophys. Res. Lett.* 30, 2095.
- World Health Organization, 2005. WHO Air Quality Guidelines for Particulate Matter, Ozone, Nitrogen Dioxide and Sulfur Dioxide: Global Update 2005: Summary of Risk Assessment. World Health Organization.
- You, H., Yang, J., Xue, B., Xiao, X., Xia, J., Jin, C., Li, X., 2021. Spatial evolution of population change in Northeast China during 1992–2018. *Sci. Total Environ.* 776, 146023.
- You, W., Zang, Z., Zhang, L., Li, Y., Wang, W., 2016. Estimating national-scale ground-level PM_{2.5} concentration in China using geographically weighted regression based on MODIS and MISR AOD. *Environ. Sci. Pollut. Res. Int.* 23, 8327–8338.
- Yu, X., Cheng, T., Chen, J., Liu, Y., 2006. A comparison of dust properties between China continent and Korea, Japan in East Asia. *Atmos. Environ.* 40 (30), 5787–5797.
- Zhang, J., Reid, J.S., Westphal, D.L., Baker, N.L., Hyer, E.J., 2008. A system for operational aerosol optical depth data assimilation over global oceans. *J. Geophys. Res. Atmos.* 113, D10208.
- Zhang, Q., Zheng, Y., Tong, D., Shao, M., Wang, S., Zhang, Y., Xu, X., Wang, J., He, H., Liu, W., Ding, Y., 2019. Drivers of improved PM_{2.5} air quality in China from 2013 to 2017. *Proc. Natl. Acad. Sci. U.S.A.* 116 (49), 24463–24469.
- Zhang, X., Arimoto, R., An, Z., Chen, T., Zhang, G., Zhu, G., Wang, X., 1993. Atmospheric trace elements over source regions for Chinese dust: concentrations, sources and atmospheric deposition on the Loess Plateau. *Atmos. Environ.* 27 (13), 2051–2067.
- Zhang, Y.L., Cao, F., 2015. Fine particulate matter (PM_{2.5}) in China at a city level. *Sci. Rep.* 5, 14884.
- Zhu, S., Yu, C., He, C., 2020. Export structures, income inequality and urban-rural divide in China. *Appl. Geogr.* 115, 102150.